Journal of Engineering Physics and Thermophysics, Vol. 66, No. 5, 1994

PROPAGATION AND EMISSION OF A NONSTATIONARY HEAT WAVE IN AIR

I. M. Kozlov, S. L. Min'ko, and
G. S. Romanov

UDC 533.9

Numerical simulation of the dynamics of propagation and formation of the front of a nonstationary spherical heat wave in air is performed. The time dependence of the radiation of the front in the optical range of the spectrum is obtained. The existence of two phases in the propagation of a heat wave is established.

The study of the dynamics of propagation of a nonstationary heat wave in air and the formation of its front, as well as investigation of the change in time of the wave luminosity, are of great practical interest. In [1] a qualitative picture of the process of heat wave propagation in air is given based on a description of radiation transfer in the radiative heat conduction approximation. In [2, 3] the structure of a heat wave in air was investigated analytically and estimates for the velocity of its propagation were given. However, an analytical approach does not give a precise and full picture of the phenomenon, and the literature lacks results of detailed numerical calculations.

In the present work we present results of numerical simulation of the dynamics of propagation and formation of a heat wave front in air with a density $\rho = 4.19 \cdot 10^{-4}$ g·cm^{-3}. We obtained temperature profiles for the time interval bounded from below by the applicability of the quasi-stationary model of radiation transfer and from above by the instant of transition to the hydrodynamic regime of expansion of a hot region and appearance of a shock wave. We investigated in detail the structure of the heat wave front and obtained the time dependence of outgoing radiation flux in the optical spectral range.

To model a heat wave, we considered the problem of cooling and expansion of a large spherical volume with energy E_0 and radius R_0 having characteristic dimensions of dozens of meters. The expansion of the hot sphere occurred only due to the heating of cold air by radiation without regard for hydrodynamic dispersion. This means that the wave velocity D is much higher than the velocity of sound in the hot region. At a temperature above 10^5 K within the region, the radiation quanta that form the heat wave front have characteristic mean free paths from tenths of a millimeter to several centimeters [1]. Thus, the radiating front width of the spherical heat wave can be much smaller than the radius of the front. As a result, numerical simulation of the phenomenon presents difficulties, since a large-scale heat wave and a narrow front generating outgoing radiation cannot be obtained in one combined calculation because of the difference in their scales by orders of magnitude. Experience gained in simulating the luminosity of shock waves [4] suggests a resolution, namely, in a numerical description the problem of the propagation and luminosity of a heat wave should be divided into separate subproblems, each having its own spatial scale. The first is large-scale simulation of the dynamics of expansion and cooling of a hot sphere to obtain a rough distribution of temperature in the medium, and the other consists in calculation of the fine structure of the quasi-stationary heat wave front and calculation of the outgoing radiation flux in the visible range of the spectrum. Such a division of the full problem into two separate subproblems is based on the following assumptions: the fine structure of a heat wave does not influence the distribution of parameters (energy or temperature) in the interior of the heated region or, consequently, the velocity of its propagation into the surroundings; on the other hand, the temperature distribution at the wave front is quasi-stationary in time and is determined at each instant by the velocity of the front and radiation fluxes from internal layers of the heated region. To account for the spectral distribution of photons, radiation transfer was considered in the multigroup approximation for the photon spectrum.

Academic Scientific Complex "A. V. Luikov Heat and Mass Transfer Institute of the Academy of Sciences of Belarus," Minsk. Translated from Inzhenerno-Fizicheskii Zhurnal, Vol. 66, No. 5, pp. 539-546, May, 1994. Original article submitted October 5, 1992.

1062-0125/94/6605-0473$12.50

By virtue of the above comments on the difference of scales, the problem of the front structure was solved in a one-dimensional plane formulation. With such an approach, for a quasi-stationary plane heat wave the following relation is valid:

$$\rho D\varepsilon - S = \rho D\varepsilon_F - S_\infty . \tag{1}$$

To determine radiation fluxes, we used the following system of equations:

$$\mu \frac{\partial I_k}{\partial r} + \kappa_k I_k = \kappa_k I_{kp} , \quad r \geq r_0 ;$$

$$S = \sum_{k=1}^{N_g} \int_{-1}^{+1} \mu I_k \, d\mu , \quad I_{kp} = \frac{30\sigma}{\pi^4 k^4} \int_{\varepsilon_k}^{\varepsilon_{k+1}} \frac{\varepsilon^3 \, d\varepsilon}{\exp(\varepsilon/kT) - 1} . \tag{2}$$

Simultaneous use of Eqs. (1) and (2) makes it possible to determine the temperature distribution in a heat wave in the presence of boundary conditions for solving the radiation transfer equation. Moreover, it is necessary to know the wave velocity D, which enters into this system as a parameter. The boundary conditions and the velocity D should be obtained by solving the large-scale problem, whose characteristic features are small temperature gradients throughout the entire region (except for a narrow segment occupied by the heat wave front) and isotropy of radiation within the hot spherical volume [1-3]. This allows calculation of radiation transfer in the diffusion approximation together with the energy equation. Then, the system of equations can be written in spherical coordinates in the following form:

$$\frac{1}{r^2} \frac{\partial}{\partial r} (r^2 S_k) + \kappa_k U_k = \kappa_k Q_k ; \quad \frac{l_k}{3} \frac{\partial}{\partial r} (U_k) + S_k = 0 ;$$

$$\frac{\partial}{\partial t} (\rho\varepsilon) + \frac{1}{r^2} \frac{\partial}{\partial r} (r^2 S) = 0 , \quad S = \sum_{k=1}^{N_g} S_k , \quad Q = \frac{60\sigma}{\pi^4 k^4} \int_{\varepsilon_k}^{\varepsilon_{k+1}} \frac{\varepsilon^3 \, d\varepsilon}{\exp(\varepsilon/kT) - 1} . \tag{3}$$

This approximation is also valid in the region of the front because the latter is formed by high-energy quanta, for which the mean free paths are much smaller than the front width. The use of a diffusional model is not quite justified when calculating radiation transfer in the low-energy region of the spectrum, including the visible one. High anisotropy and large mean free paths of the quanta characterize this region, in view of which radiation fluxes in this spectral range were determined by solving the following radiation transfer equation:

$$\mu \frac{\partial I_k}{\partial r} + \frac{1 - \mu^2}{r} \frac{\partial I_k}{\partial \mu} + \kappa_k I_k = \kappa_k I_{kp} ; \tag{4a}$$

$$S = \sum_{k=1}^{N_g} \int_{-1}^{+1} \mu I_k \, d\mu , \quad k = 1, \ldots, N_g . \tag{4b}$$

As already noted, to solve the problem concerning the structure of a quasi-stationary plane wave, it is necessary to know the heat wave velocity. The heat wave velocity is understood to be the velocity of that point of the front at which the temperature gradient is maximum. Within the framework of the large-scale problem, the front represents an infinitely thin portion of a heat wave with air heated by radiation on one side and cold air on the other. With this approximation the following relation is valid at the wave front:

$$\rho\varepsilon D = S . \tag{5}$$

Here S is the radiation flux that heats up the cold air. In solving problem (3), the angular distribution of the radiation intensity at the wave front was calculated at the needed times as boundary conditions for problem (1), (2). In this case Eq. (4a) was solved for $0 < \mu \leq 1$ using the energy distribution obtained from Eq. (3). Thus, a closed system of equations is obtained to simulate the problem at hand.

The thermodynamic properties of air in the range of specific internal energies $0.37 - 2.5 \cdot 10^4$ kJ/g were tabulated [5] in the form of the functional relation

$$\log T = f(\ln \rho\,,\ \ln \varepsilon)\,.$$

For energy values below and above the limits indicated, the ideal gas equation of state was used for a cold and a fully ionized air, respectively.

The optical properties of air are also tabulated in the multigroup approximation in the form of the functional relation

$$\ln \kappa_{ijk} = f(\ln \rho_i\,,\ \ln T_j\,,\ k)\,,$$

$$i = 1\,,\ \ldots\,,\ 11\,;\quad j = 1\,,\ \ldots\,,\ 39\,;\quad k = 1\,,\ \ldots\,,\ N_g\,.$$

The spectral properties of the medium were accounted for in the 14-group approximation: 0.0155 – 0.511 – 1.41 – 2.72 – 4.51 – 6.52 – 7.95 – 9.96 – 18.6 – 80.6 – 248 – 398 – 2300 – 6000 – 20,000 eV. Use was made of absorption coefficients averaged within the indicated limits, following both Planck and Rosseland. Tables of coefficients were determined for temperature values within the range from 0.03 to 1778 eV. For low temperatures 0.03 – 2 eV they were obtained from data of [6], while for those above 2 eV the coefficients for air were taken from [7]. Data on the basis of which tables were compiled for 17 groups in the optical range were taken from [6]. These data were matched with the tables of absorption coefficients presented in [7] for temperatures within the range from 2 to 1778 eV. The width of each group in the optical range amounted to 0.1 eV, and the boundaries of the range for the energies of the quanta were 1.5 and 3.25 eV.

Calculation of the diffusional system of radiation transfer equations (3) was made using a scheme obtained by matching local analytical solutions of diffusion equations at the nodes of a spatial grid for optically homogeneous cells, assuming linearity in space for the temperature portion of the radiation sources Q. Hereafter, we will omit subscripts indicating the spectral group to which a quantity belongs. We will use only grid indices, denoting thereby the numbers of the cells for optical coefficients and grid steps. For the remaining quantities, subscripts show the numbers of the nodes at which these quantities are determined. Then, the system of linear equations for a numerical solution of the diffusion equations in index-vector notation takes the form

$$\exp(-\gamma_{j-1} h_{j-1})\, A_j \mathbf{X}_{j-1} - B_j \mathbf{X}_j + \exp(-\gamma_j h_j)\, C_j \mathbf{X}_{j+1} = -\mathbf{F}_j\,, \tag{6}$$

$$j = 1\,,\ 2\,,\ \ldots\,,\ N\,,$$

where

$$\mathbf{X}_j = \begin{pmatrix} \sqrt{3}\, S_j \\ U_j \end{pmatrix},\quad A_1 \equiv \begin{pmatrix} 0 & 0 \\ 0 & 0 \end{pmatrix},\quad C_N \equiv \begin{pmatrix} 0 & 0 \\ 0 & 0 \end{pmatrix};$$

$$A_j = \begin{pmatrix} \left(\dfrac{\beta}{\gamma}\right)_{j-1} G_0(\gamma_{j-1} r_{j-1}) & G_1(\gamma_{j-1} r_{j-1}) \\ 0 & 0 \end{pmatrix};$$

$$B_j = \begin{pmatrix} \left(\frac{\beta}{\gamma}\right)_{j-1} \left(\frac{r_j}{r_{j-1}}\right)^2 G_0(\gamma_{j-1} r_j) & \left(\frac{r_j}{r_{j-1}}\right)^2 G_1(\gamma_{j-1} r_j) \\ -\left(\frac{\beta}{\gamma}\right)_j H_0(\gamma_j r_j) & H_1(\gamma_j r_j) \end{pmatrix};$$

$$C_j = \begin{pmatrix} 0 & 0 \\ -\left(\frac{\beta}{\gamma}\right)_j H_0(\gamma_j r_{j+1}) & H_1(\gamma_j r_{j+1}) \end{pmatrix};$$

$$\mathbf{F}_j = \begin{pmatrix} F_{j1} \\ F_{j2} \end{pmatrix}; \quad F_{j1} = Q_j \left(\frac{r_j}{r_{j-1}}\right)^2 G_1(\gamma_{j-1} r_j) - Q_{j-1} \exp(-\gamma_{j-1} h_{j-1}) \times$$

$$\times G_1(\gamma_{j-1} r_{j-1}) + (Q_{j-1} - Q_j) \Phi(\gamma_{j-1} r_{j-1}, \gamma_{j-1} r_j);$$

$$F_{j2} = Q_j H_1(\gamma_j r_j) - Q_{j+1} \exp(-\gamma_j h_j) H_1(\gamma_j r_{j+1}) + (Q_{j+1} - Q_j) F(\gamma_j r_j, \gamma_j r_{j+1}).$$

Here the following symbols are introduced:

$$\gamma = \sqrt{\left(\frac{3\kappa}{l}\right)}, \quad \beta = \frac{\sqrt{3}}{l};$$

$$\Phi(\chi_1, \chi_2) \equiv \frac{\exp(-\chi_2)}{\chi_1^2 (\chi_2 - \chi_1)} \int_{\chi_1}^{\chi_2} \sqrt{\left(\frac{\pi}{2\chi}\right)} I_{3/2}(\chi) \chi^2 \, d\chi;$$

$$F(\chi_1, \chi_2) \equiv \frac{\exp(\chi_1)}{(\chi_2 - \chi_1)} \int_{\chi_1}^{\chi_2} \sqrt{\left(\frac{2}{\pi\chi}\right)} K_{3/2}(\chi) \chi^2 \, d\chi$$

$$G_n(\chi) \equiv \sqrt{\left(\frac{\pi}{2\chi}\right)} \exp(-\chi) I_{n+1/2}(\chi);$$

$$H_n(\chi) \equiv \sqrt{\left(\frac{2}{\pi\chi}\right)} \chi^2 \exp(\chi) K_{n+1/2}(\chi), \quad n = 0, 1,$$

where $I_\lambda(\chi)$ and $K_\lambda(\chi)$ are modified Bessel functions.

System of equations (6) was solved by matrix fitting:

$$\mathbf{X}_j = D_{j-1} \mathbf{X}_{j-1} + \mathbf{E}_{j-1}, \quad j = 1, 2, \ldots, N.$$

The fitting coefficients (matrices $\mathbf{D}_j$ and vectors $\mathbf{E}_j$) were calculated from the recurrence formulas

$$D_{j-1} = \exp(-\gamma_{j-1} h_{j-1}) (B_j - \exp(-\gamma_j h_j) C_j D_j)^{-1} A_j;$$

$$\mathbf{E}_{j-1} = (B_j - \exp(-\gamma_j h_j) C_j D_j) (\mathbf{F}_j + \exp(-\gamma_j h_j) C_j \mathbf{E}_j),$$

$$j = 1, 2, \ldots, N.$$

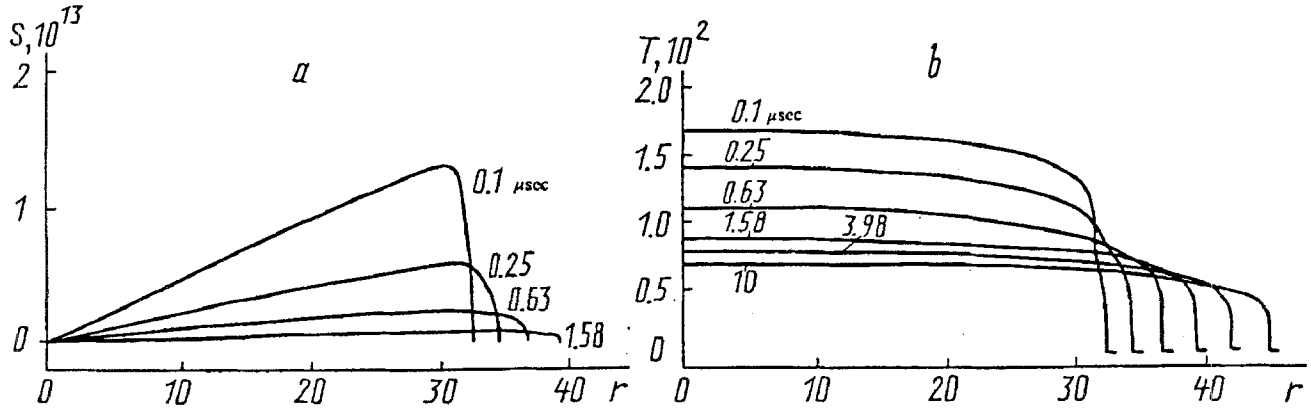

Fig. 1. Spatial distribution of the radiation flux density (a) and the temperature (b) for different instants of time. S, W·cm^{-2}; T, eV; r, m.

The mean group coefficients of absorption were represented by the Planck mean spectral coefficients of absorption for air, and the coefficients l are the Rosseland mean free paths in the corresponding spectral groups.

The kinetic radiation transfer equations for solving problems (4a) and (4b), as well as for obtaining the outgoing radiation flux in the visible range from the available temperature profiles at the heat wave front, were solved numerically by the method of characteristics. For this purpose, we used the integral solution of the equation along the beam between the nodes (points at which the beam intersects the grid surfaces bounding a cell space). Just as in calculating radiation diffusion, we assumed homogeneity of the optical properties of the medium along the beam between neighboring nodes and linearity of the distribution of sources along the beam over this segment. The latter assumption allows the solution to reach the limiting regime of energy transfer – radiative heat conduction in an optically thick medium. The radiation intensity from node to node along a characteristic was calculated using the following formula:

$$I_{j+1} = I_j \exp(-\kappa_{pj}\Delta x_j) + 0.5\,(I_{pj+1} + I_{pj}) + 0.5\,(I_{pj+1} - I_{pj}) \times$$

$$\times \left(1 + \exp(-\kappa_{Rj}\Delta x_j) - 2\,(1 - \exp(-\kappa_{Rj}\Delta x_j)\,(\kappa_{Rj}\Delta x_j))^{-1}\right).$$

Radiation transfer in problem (4a), (4b) was calculated on 10 characteristics corresponding to a grid over the angle with nodes selected as follows:

$$\mu = \cos\left(\frac{\pi}{20}(i-1)\right), \quad i = 1, 2, \ldots, 10.$$

Radiation energy fluxes were calculated assuming a linear character for the dependence of the intensity over the cosine μ of the angle in the regions between the nodes.

In numerically solving Eq. (1) to determine the parameter D, which, as noted above, is not involved explicitly in Eq. (3), we used a mobile spatial grid. In this grid, the velocities of the nodes are determined from the condition that the cells are most insensitive to radiation energy transfer, which approximately corresponds to satisfaction of the equality $\rho\varepsilon V - S = 0$ for the grid nodes in the disturbed region. After a certain interval of time from the start of a calculation on this grid the solution becomes steady and the propagation of the heated region relative to the cells of the grid ceases. This approach to solving problems of propagation of heat waves permits one to avoid unwanted effects associated with jumpwise propagation of disturbances in going from one cell to another on fixed grids. Simultaneously it offers an efficient means of determining the velocity of the front, which is assumed in this case to be equal to that of the grid node with the value r_0 and for which condition (5) is satisfied.

Problem (3), (4a), (4b) was solved numerically, on 70 cells of a spatial grid with progressive compression of the grid in the vicinity of the wave front. System of equations (1)-(2) was solved by an iteration procedure on

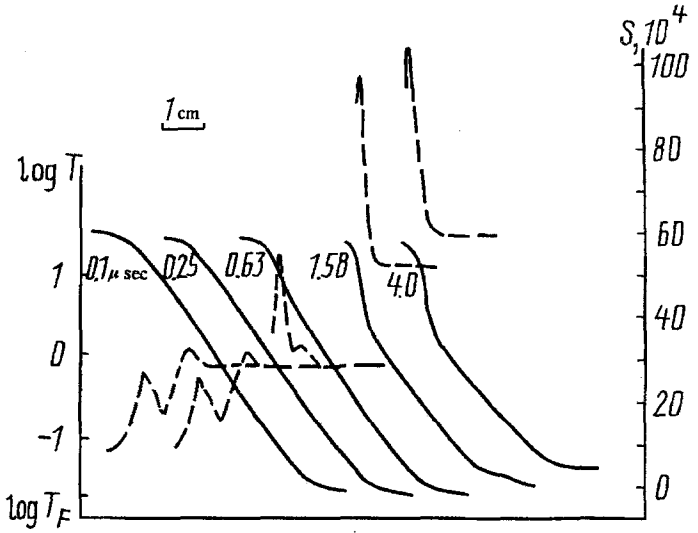

Fig. 2. Distribution of the temperature (solid lines) and the radiation fluxes (dashed lines) at the heat wave front. log T, eV.

a spatial grid consisting of 451 nodes. The distribution of the nodes on the grid was rearranged so that the optical thicknesses of the cells for outgoing radiation, which are located in the region of generation of the latter, did not exceed unity.

The results of calculations for the dynamics of the propagation of a heat wave and for the formation of its front in air are presented in Figs. 1-3. The dependence of the radiation energy flux on time is shown in Fig. 4. The initial values of the energy and the radius of the hot sphere were selected such that the temperature within the region could substantially exceed 10^5 K. For the above-indicated limitations the time interval was equal to 0.1 – 10 μsec.

The entire space heated by radiation can be divided into three portions (Fig. 1). A transparent region is located in the interior of the hot volume. The temperature in this region behaves in line with the well-known behavior in the case of radiative heat conduction. The change in radiation flux is close to a linear law and increases from zero at the center to its maximum value on the boundary. The region of the front represents a portion of the heat wave where the temperature falls almost to the background value and its gradient is maximum. Next is the region of the heating tongue – the zone of heating by nonequilibrium radiation – which penetrates far into the cold air. The region is formed as a result of absorption of hard quanta of nonequilibrium radiation by the substance. The character of heating ahead of the front is similar to heating in the zone ahead of strong shock waves in air [4]. This resemblance is not accidental, since the nature of the processes occurring at the front of both types of waves is the same. In Fig. 2 spatial temperature profiles in the region of the heat wave front and the corresponding profiles of the radiation energy flux in the visible portion of the spectrum are presented for a sequence of instants of time. From Figs. 2 and 3 it is seen that the region of the front can, in turn, be divided into two parts: the wave front proper where radiation is close to the equilibrium one and the tongue of heating by hard radiation. For late instants of time the boundary between them is rather distinguishable. For early instants of time this boundary occurs in the region of the local minimum on the radiation flux profile.

Figure 3 presents a hodograph and the time dependence of the heat wave velocity. We can see that, just as for the classical wave with nonlinear heat conduction, they are close to a power law.

Let us consider in more detail the dynamics of the propagation and formation of the heat wave front in our problem. During the first microsecond, intense cooling of the internal hot region from 170 to 100 eV occurs mainly due to rapid expansion and a substantial increase in the cold air volume heated by radiation. The energy emitted by the sphere at this instant is small. During the remaining 9 μsec the intensity of cooling is much lower although the quantity of energy produced by emission is much higher, since by this instant of time the inflow of energy into the region of the front has decreased because of the cooling of the inner hot layers and the wave velocity has decreased almost tenfold. The temperature fell from 100 to 75 eV. From 0.1 to 0.9 μsec the temperature profile of

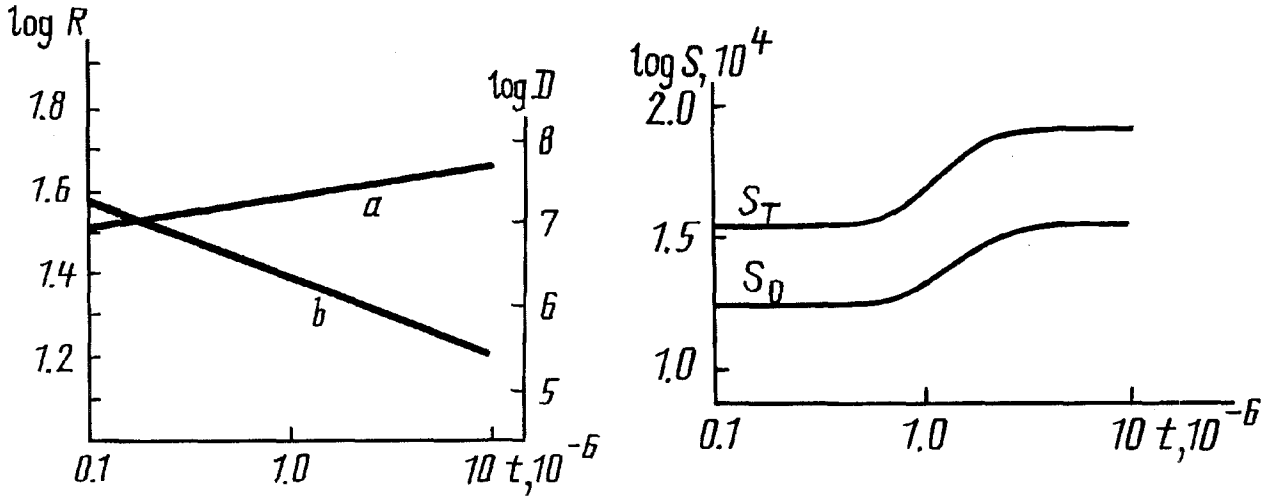

Fig. 3. Hodograph (a) and time dependence of the velocity (b) of a heat wave. log R, m; log D, m·sec^{-1}; t, sec.

Fig. 4. Time dependence of the outgoing radiation flux: S_T, total flux; S_0, in

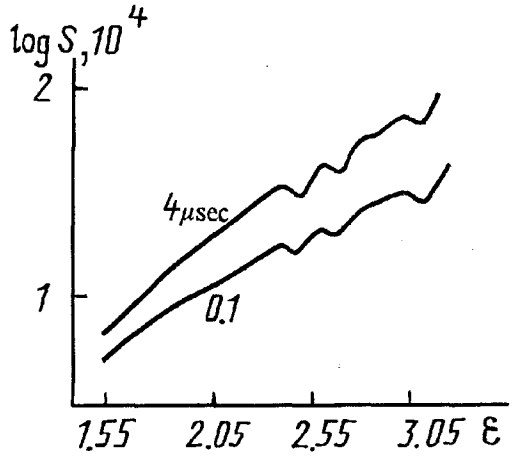

Fig. 5. Spectral distribution of the outgoing radiation flux in the visible range for two instants of time. log S, W·cm^{-2}·eV^{-1}.

the front has a virtually unchanged steepness, and the outgoing radiation flux remains almost constant. On the radiation flux profile in the region of the front we can clearly see a second local maximum, which is located in the region where the outgoing radiation of the visible range is generated. With time it is displaced into the region with a sharply changing temperature, thus increasing the outgoing radiation flux. In the next 0.2 μsec a sharp increase in the steepness of the front in the high-temperature region takes place. The local minimum disappears, and the first maximum becomes much higher than the second and, expanding, absorbs the latter. Thus, the flux generated in the region of radiation emission is augmented with the flux from the high-temperature region of the front. Precisely this leads to growth of the outgoing radiation flux. Thereafter, in the course of 1.1 -10 μsec the structure of the front changes little, mainly in the zone of the heating tongue. We can clearly see in Fig. 3 that with time the heating tongue extends father into the cold air region. This is due to the fact that because of the increased steepness of the high-temperature portion of the profile the tongue itself became more transparent for hard radiation, which, as already noted, plays a major part in the formation of the tongue. In this phase the main energy loss by the sphere occurs in the visible spectral range: 84% of the total energy (at the time 10 μsec) carried away by radiation to "infinity." The distribution over the spectrum in the visible region for two instants of time is shown in Fig. 5. It should be noted that the greatest change in time occurs for the violet edge of the spectrum of the visible region.

The numerical investigation carried out allowed the conclusion that there are two phases in the propagation of a spherical nonstationary thermal radiation wave in air, with each having its specific features in the distribution of parameters at the wave front. The characteristic time of the first phase is practically an order of manitude smaller than that of the second. The time of transition from one phase to the other is much smaller than the characteristic time of the first phase. The calculation confirmed the assumption that the fine structure of a heat wave does not influence the temperature (energy) distribution within the heated region, i.e., does not influence the velocity of propagation of heat to the surrounding space, as well as the assumption that the temperature distribution at the front at each instant of time is determined by the velocity of the front and radiation fluxes from within the heated region.

NOTATION

D, heat wave velocity; ρ, air density; ε, specific internal energy of the medium; T, absolute temperature; ε_k, boundaries of the energy groups of the quanta; S, radiation flux; I, radiation intensity increased 2π times; μ, cosine of the angle; k, Boltzmann constant; σ, Stefan-Boltzmann constant; S_∞, radiation flux "at infinity"; U, equilibrium radiation density; κ, absorption coefficient with regard for forced emission; l, mean free path of the quanta; c, velocity of light in vacuum; Δx_j, length of the portion of a characteristic between the j-th and $(j+1)$-th nodes; κ_P and κ_R, Plank and Rosseland mean group radiation absorption coefficients; r, radial coordinate; r_0, radius at which the boundary conditions are determined. Subscripts F, background quantities; k, index of the spectral group; N_g, number of spectral groups.

REFERENCES

1. Ya. B. Zel'dovich and Yu. P. Raizer, Physics of Shock Waves and High-Temperature Hydrodynamic Phenomena [in Russian], Moscow (1978).
2. A. S. Kompaneets and E. Ya. Lantsburg, Zh. Éksp. Teor. Fiz., **41**, 1649 (1961).
3. A. S. Kompaneets and E. Ya. Lantsburg, Zh. Éksp. Teor. Fiz., **43**, 234 (1962).
4. J. Zinn and R. C. Anderson, Phys. Fluids, **16**, No. 10, 1639 (1973).
5. N. M. Kuznetsov, Thermodynamic Functions and Shock Adiabats of Air at High Temperatures [in Russian], Moscow (1965).
6. I. V. Avilova, L. M. Biberman, V. S. Vorob'yov, et al., Optical Properties of Hot Air [in Russian], Moscow (1970).
7. S. I. Kas'kova, G. S. Romanov, L. K. Stanchits, et al., Zh. Prikl. Spektr., **49**, No. 1, 160 (1988).